粉末床熔融的多材料铺粉过程中粉末扩散的数值研究

Wang, Lin; Li, Erlei; Zhou, Zongyan; Zhang, Baicheng; Yu, Aibing

DOI
10.1007/s10409-022-22255-x

Publication date
2023

Document Version
Final published version

Published in
Acta Mechanica Sinica/Lixue Xuebao

Springer

Acta Mechanica Sinica

CrossMark click for updates

• RESEARCH PAPER •

Acta Mech. Sin., Vol. 39, 722255 (2023)
https://doi.org/10.1007/s10409-022-22255-x

Simulation of powder spreading of functionally graded materials in powder bed fusion additive manufacturing

Lin Wang[1,2], Erlei Li[1], Zongyan Zhou[1,3*], Baicheng Zhang[4], and Aibing Yu[1]

[1] *ARC Hub for Computational Particle Technology, Department of Chemical & Biological Engineering, Monash University, Clayton VIC 3800, Australia;*

[2] *Delft University of Technology, Stevinweg 1, 2628 CN, Delft, The Netherlands;*

[3] *Jiangxi Provincial Key Laboratory for Simulation and Modelling of Particulate Systems, Jiangxi University of Science and Technology, Nanchang 330013, China;*

[4] *Beijing Advanced Innovation Center Materials Genome Engineering, Advanced Material & Technology Institute, University of Science and Technology Beijing, Beijing 100083, China*

Received September 15, 2022; accepted November 9, 2022; published online January 9, 2023

Powder bed fusion additive manufacturing has been applied to the fabrication of functionally graded materials. A new design that allows the material composition to change along the direction perpendicular to the powder spreading has been reported in the literature. Based on this design, this work examines the quality of the graded spread powder layer with two powders, which have a large difference of density. The results reveal that during the spreading of graded powders, the volume of particles on the heavy powder side is deposited less than that on the light powder side, indicating that heavy particles diffuse to the light powder side. This diffusion is affected by the spreading speed, but not much by the layer gap. Large spreading speed causes more significant deviation. The results also show that particle size affects diffusion, indicating that decreasing the particle size of the heavy powder may be a solution to reduce diffusion.

Powder spreading, Powder bed fusion additive manufacturing, Functionally graded material, DEM simulation

Citation: L. Wang, E. Li, Z. Zhou, B. Zhang, and A. Yu, Simulation of powder spreading of functionally graded materials in powder bed fusion additive manufacturing, Acta Mech. Sin. **39**, 722255 (2023), https://doi.org/10.1007/s10409-022-22255-x

1. Introduction

Functionally graded materials (FGMs) are novel composite materials in which compositions or structures vary gradually along certain directions. The parts can then present different properties at different positions of the parts [1-3]. Meanwhile, the boundaries between different materials and the delamination phenomenon within a traditional composite material are eliminated [4,5]. Therefore, FGMs are receiving more attention in many fields such as aerospace, nuclear power, sensors, biomedical implants and optoelectronic devices [1]. For the fabrication of FGMs, conventional manufacturing (CM) methods, including bulk processing methods and coating methods, are generally used in industrial production [6]. Theoretically, the additive manufacturing (AM) method [7] can allow more flexible product geometries and more complicated gradients of material compositions than CM, which can unlock the potential of FGMs [7-9]. However, the fabrication of FGMs via AM is still in the laboratory research rather than industrial production [1]. More studies need to be carried out to make the FGM structures more controllable.

Among various AM methods, selective laser melting (SLM) and electron beam melting (EBM) are suitable for the fabrication of functional metal parts due to the fact that the melting and re-solidification of metal materials can result in denser parts with enhanced mechanical properties [7,10,11]. Several studies have been conducted to manufacture different FGMs via powder bed fusion (PBF), for example, the parts with either graded structures [12-18] or graded material

*Corresponding author. E-mail address: zongyan.zhou@jxust.edu.cn (Zongyan Zhou)
Executive Editor: Xiaoyan Ye

compositions [19-22]. In PBF, powder materials are first spread horizontally to form a powder layer, and then the selected regions in the layer are melted by energy beams and re-solidify. The parts are gradually fabricated along the vertical direction by repeating the powder spreading and layer melting [7]. For the fabrication of FGMs, the material composition varies from layer to layer. This requires the preparation of a large number of powder mixtures with different powder compositions. This makes the fabrication process less efficient. Due to this limitation, the material gradient so far in the part is generally discrete and simple [2,19-22].

To overcome this difficulty, Wen et al. [23] proposed a new strategy for the fabrication of FGMs via PBF. In this method, a powder mixture is prepared with the composition varying along one direction (e.g., the horizontal direction of y), which is perpendicular to the powder spreading direction (e.g., the horizontal direction of x). Then, the parts with a material gradient varying along the y-direction can be fabricated. This method has the advantage that there is no need to prepare different powder mixtures. However, to ensure the quality of the parts, the material gradient distribution of the spread powder layer along the y direction needs to be consistent with the gradient distribution in the initial powder pile. But note that for granular mixtures, segregation can occur due to the difference in particle sizes or densities. This can lead to the varied material gradient distribution of the powder layer during the spreading process. However, the studies for the possible size- or density- induced segregation for producing gradually graded materials by AM have not been well reported in the literature.

In this work, the density-induced segregation during powder spreading is examined, focusing on the variation of the material gradient distribution in the powder layer from the one in the initial powder pile. Two types of powder are selected: powder Ta and powder Ti, which have a significant difference in density. The Ta-Ti-alloy can obtain both corrosion resistance and mechanical properties, and the parts with graded Ta and Ti components can possess outstanding corrosion resistance on the Ta side and outstanding mechanical properties on the Ti side. In the simulation, the powder spreading starts with the preparation of the initial powder pile with the material composition changing linearly from 100% (volume fraction) Ta to 100% (volume fraction) Ti along the y-direction perpendicular to the spreading x-direction. After the spreading, the material composition distribution along the y-direction is analyzed in detail. The effect of powder size ratios is also examined for further understanding of the segregation mechanism.

2. Mathematical model

The discrete element method (DEM), initially proposed by Cundall and Strack [24], has been widely used to study powder spreading in PBF AM. In this work, the DEM simulation is based on LIGGGHTS [25] and LAMMPS [26] codes. Based on Newton's second law, the translational and rotational motions of a particle are respectively given by

$$m_i \frac{\mathrm{d}\mathbf{v}_i}{\mathrm{d}t} = \mathbf{F}_n + \mathbf{F}_t + \mathbf{F}_a, \tag{1}$$

$$I_i \frac{\mathrm{d}\boldsymbol{\omega}_i}{\mathrm{d}t} = \mathbf{T}_t + \mathbf{T}_r, \tag{2}$$

where m_i, I_i, $\mathbf{v}_i$ and $\boldsymbol{\omega}_i$ are the mass, moment of inertia, velocity and angular velocity of particle i respectively. The forces acting on particle i include normal contact force $\mathbf{F}_n$ and tangential contact force $\mathbf{F}_t$ if the particles are contacting, and also the non-contact van der Waals force $\mathbf{F}_a$. The torque on particle i includes both the torque from the tangential contact force and the torque resulting from rolling friction. More details of the DEM model and force/torque equations can be referred to Refs. [27,28].

In particular, the adhesion force between particles is represented by van der Waals attraction force, which is the integrated expression of Lennard-Jones potential between atoms. It is the intrinsic force between matters whose magnitude is determined by the material. According to Ref. [29], van der Waals attractive potential between two particles is given by

$$U_A = -\frac{H}{6}\left\{\frac{2r_i r_j}{d^2-(r_i+r_j)^2} + \frac{2r_i r_j}{d^2-(r_i-r_j)^2} + \ln\left[\frac{d^2-(r_i+r_j)^2}{d^2-(r_i-r_j)^2}\right]\right\}, \tag{3}$$

where H is the Hamaker constant which determines the force magnitude, and d is the distance between particle centers. For coarse particles, van der Waals force is ignored because it is extremely small compared with gravity. While for microparticles, van der Waals force is important in governing particle packing and flow behaviors.

Note that the calibration of DEM parameters and the model validation have been conducted in our previous work [27]. Sliding friction coefficient and Hamaker constant are identified as the critical parameters in DEM simulation. By varying these parameters and matching the simulated packing density and the angle of repose to those from experiments, proper material parameters used in DEM were obtained. This work employs these verified parameters and the validated DEM model to study the powder spreading for FGMs.

3. Simulation conditions

The material properties of the two powders except density are assumed to have the same values as those used in the previous work [28], which are calibrated based on Ni-alloy powder [27]. Table 1 lists the parameters used in this work.

Two types of powder are employed: powder Ta and powder Ti. It is assumed that both powders have the same size distribution, with the diameter varying from 15 μm to 45 μm and the D50 = 30 μm. In the simulation (Fig. 1a and b), the width of the initial powder pile along the y direction is 3000 μm, and a total of 106660 particles are used (including 53330 Ta particles and 53330 Ti particles). The composition of the powder pile changes from 100% Ta at y = 0 μm to 100% Ti at y = 3000 μm (Fig. 1c). In the middle of y = 1500 μm, the powder has 50% Ta and 50% Ti. For convenience, the side of the powder pile at y < 1500 μm is called the heavy powder side (Ta), and the side at y > 1500 μm is called the light powder side (Ti) in this work.

Note that the initial powder pile is obtained by the random generation of particles in a rectangular box. To achieve the required powder gradient distribution (Fig. 1c), a probability varying from 0 to 1 along the y direction determines whether a generated particle is kept or deleted according to its position on the y axis. After the packing, the side walls of the box are removed, then a vertical blade spreader moves horizontally along the +x direction to spread the initial powder pile to form a powder layer on the underlying part. The underlying part and the spreader have the same physical properties as particles. Note that the underlying part is a plane with a large sliding friction coefficient of 0.9 to mimic the rough surface of the part. In the simulation, different spreading speeds (e.g., the moving velocity of the blade) and layer gaps (e.g., the gap between the bottom of the blade and the underlying part) are used and shown in Table 1.

4. Results and discussion

4.1 Deposited powder volume in the y direction

Figure 2 shows the top view of a section of the spread powder layer with a spreading speed of 0.05 m/s and a layer gap of 70 μm. The black arrow points to the spreading direction. Along the +y direction, the volume fraction of Ta particles (red) decreases from 100% to 0, and the volume fraction of Ti particles (blue) increases from 0 to 100%. Generally, the powder layer has a good gradient composition distribution in the +y direction, but it needs to be analyzed quantitatively and the results are shown in Figs. 3 and 4.

Figure 3 quantitatively shows the variation of the deposited volume of particles per unit area in the +y direction. In the analysis, a region in the powder layer with a length of

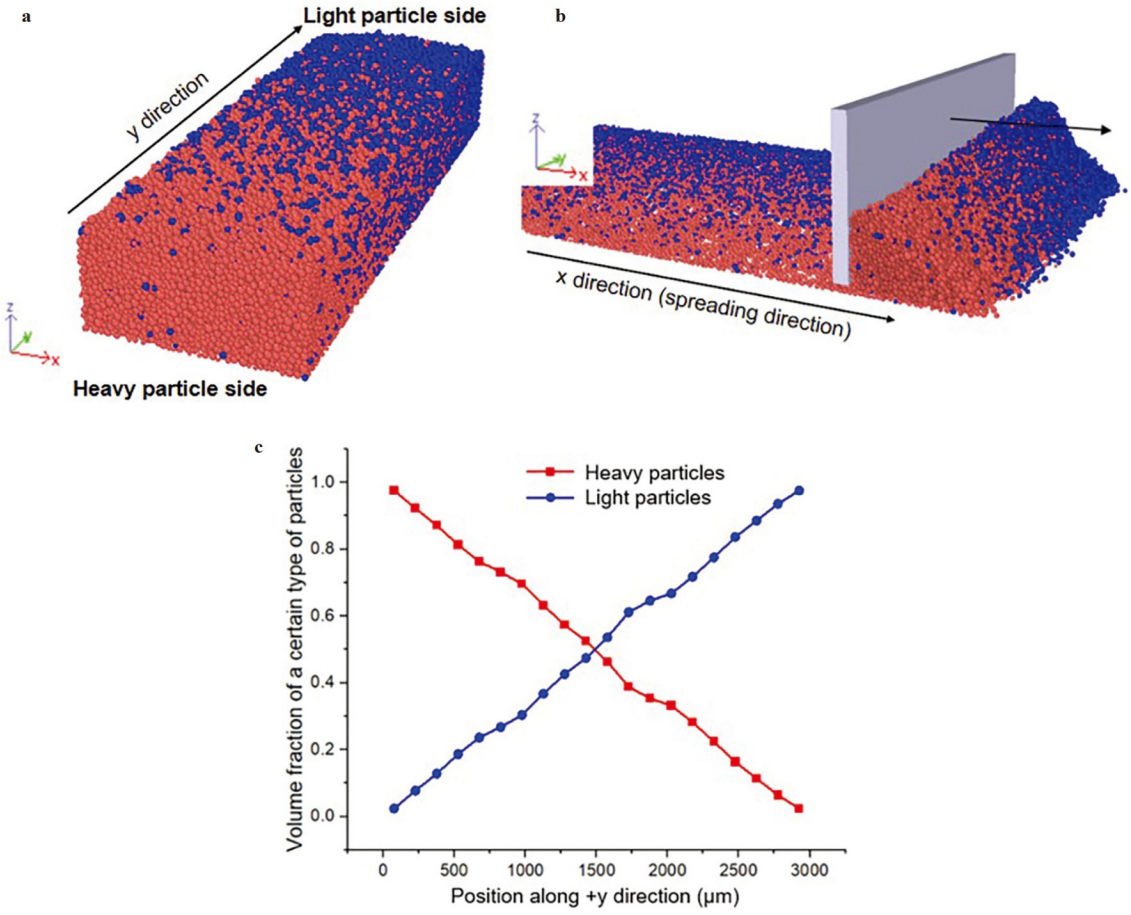

Figure 1 **a** Generation of the initial powder pile in a rectangle box, **b** powder spreading process by a blade, and **c** volume fraction of each powder along the y direction in the initial powder pile. Note that red particles are powder Ta and blue particles are powder Ti.

Table 1 Parameters used in the DEM simulation

Parameter	Value
Hamaker constant, H (J)	1×10^{-20}
Sliding friction coefficient, μ_s	0.3
Rolling friction coefficient, μ_r	0.005
Particle diameter (μm)	15-45
Particle density (g/cm^3)	16.7 (Ta); 4.51 (Ti)
Young's modulus, Y (Pa)	10^9
Restitution coefficient, e	0.35
Poisson's ratio, v	0.3
Spreading speed (m/s)	0.025-0.15
Layer gap (μm)	30-130

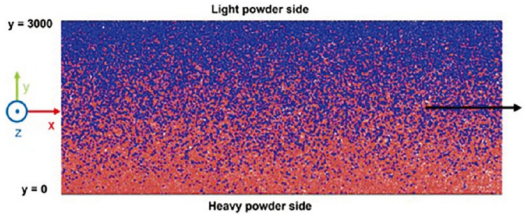

Figure 2 Top view of the spread powder layer with the distribution of each powder when the spreading speed is 0.05 m/s and the layer gap is 70 μm.

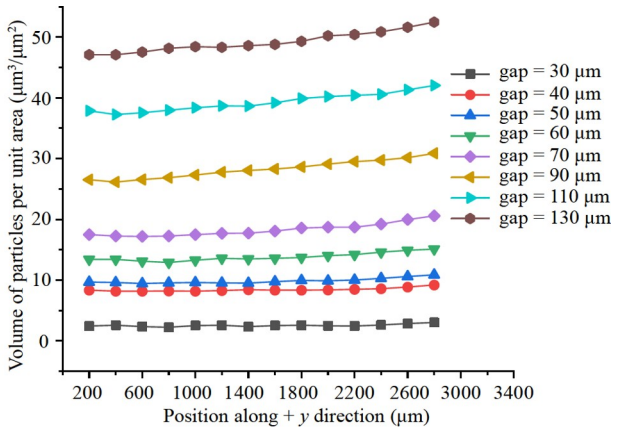

Figure 3 Variation of the deposited particle volume along the y direction when the spreading speed is 0.05 m/s.

8000 μm along the spreading direction is selected. The beginning of the region is 4000 μm from the initial powder pile. It can be observed that the deposited particle volume increases slightly from the heavy powder side (Ta) to the light powder side (Ti). With the layer gap increasing, more powder is deposited, and the diffusion of heavy particles to the light powder side is more obvious.

Figure 4 further shows the variation of the deposited volume of each powder in the y direction under different conditions. Note that for different spreading speeds, the layer gap is fixed at 50 μm; for different layer gaps, the spreading speed is fixed at 0.05 m/s. In figures, the middle position along the $+y$ axis is y = 1500 μm, and the two dashed lines are at y = 1400 and 1600 μm, respectively. It is shown that the gradient distribution of the material composition is different from that in the initial powder pile. For example, except the case of the low spreading speed at 0.025 m/s, along the y direction, the position (e.g., the intersection point of two curves) where heavy particles and light particles have the same volume is on the light particle side (Fig. 4a). At the middle position (y = 1500 μm), the volume fraction of heavy particles is expected to be 50% (see Fig. 1c, for example), while it is larger than 50%. This means that at higher spreading speed (e.g., larger than 0.05 m/s), heavy particles diffuse to the light powder side during the spreading process. Note that at the low spreading speed of 0.025 m/s, the result is opposite. This indicates that the spreading speed is an important parameter in affecting the diffusion of particles. For the effect of the gap, as shown in Fig. 4b, the deviation is not affected much when the spreading speed is fixed (e.g., 0.05 m/s).

The phenomenon of the diffusion of particles from the heavy powder side to the light powder side at a higher spreading speed occurs at the beginning of the spreading, which changes the gradient distribution along the y direction. According to Chen et al. [30], the efficiency of particle deposition through the gap between the bottom of the vertical blade spreader and the underlying part is determined by the strength of the force chains in front of the spreader and connecting the spreader bottom and the underlying part. For particles with larger density, the flow in front of the spreader bottom, as illustrated in our previous work [28], must be slower, resulting in stronger force chains. The deposited particle volume with more heavy particles is thus smaller than the deposited particle volume with less heavy particles. Therefore, without the migration of particles from the heavy powder side to the light powder side at the very beginning, the gradient distribution in the powder layer should still deviate from the initial pile. It should be noted that with the spread speed decreasing, the diffusion of heavy particles to the light powder side weakens. This suggests that the diffusion or the deviation could be controlled by employing a proper spreading speed.

4.2 Variation of powder pile properties along the x direction

The phenomenon of the deposited particle volume difference in the y direction could be closely related to the size of the powder pile. Here, the variation of the pile volume in different regions of the powder pile with spreading distance is calculated and shown in Fig. 5a. Note that the powder pile is divided into 5 regions in the y direction, where Region 1 is on the heavy powder side, and Region 5 is on the light powder side. It can be observed that for the initial powder pile (at x = 0), the volume of the powder pile from the heavy

powder side (Region 1) to the light powder side (Region 5) remains constant. Once the spreading begins, the volume on the light powder side instantly becomes larger than that on the heavy powder side. After the spreading distance exceeds 4000 μm, the differences between different regions remain constant. It is inferred that when the difference in the volume of the powder pile between the heavy and light powder sides reaches a certain value, the weight difference is not large enough to cause further particle flow from the heavy powder side to the light powder side.

Figure 5b shows the variation in the corresponding mass of different sections of the powder pile. It can be inferred that the difference in weights of the heavy powder pile and light powder pile causes the flow of particles in the powder pile from the heavy powder side to the light powder side. The flow can be reflected by the velocity of particles along the y direction, as shown in Fig. 5c. Before the spreading distance of 5000 μm, particles in each section of the powder pile possess velocities along the $+y$ direction. After 5000 μm of spreading, the velocities decrease to nearly 0. As previously discussed, the flow does not cause particle size segregation. When the flow reaches a certain extent, the weight difference is not large enough to cause particle flow to the light side. The larger height of the powder pile on the light powder side also prevents particle flow. It should be noted that in this work, the width of the system along the y direction and the scale of the powder pile are both limited. The relationship between these parameters and the above phenomenon is worth future study.

4.3 Effect of particle size distribution

The simulation cases above assume that both powders of Ta and Ti have the same particle size distribution. In this section, we examine how the particle size difference between Ta and Ti powder affects the spreading behavior. Two graded powder mixtures are used: the mixture of 30 μm Ta and 20 μm Ti, and the mixture of 40 μm Ta and 20 μm Ti. Figure 6 shows the deposited particle volume for each material and the volume variation along the y direction. It can be observed that compared with Fig. 4, the particle volume of the powder layer on the light particle side is further larger than that on the heavy powder side. The position (e.g., the intersection point) where heavy particles and light particles have the same deposited particle volume deviates more from the middle position. This indicates that for the spreading of

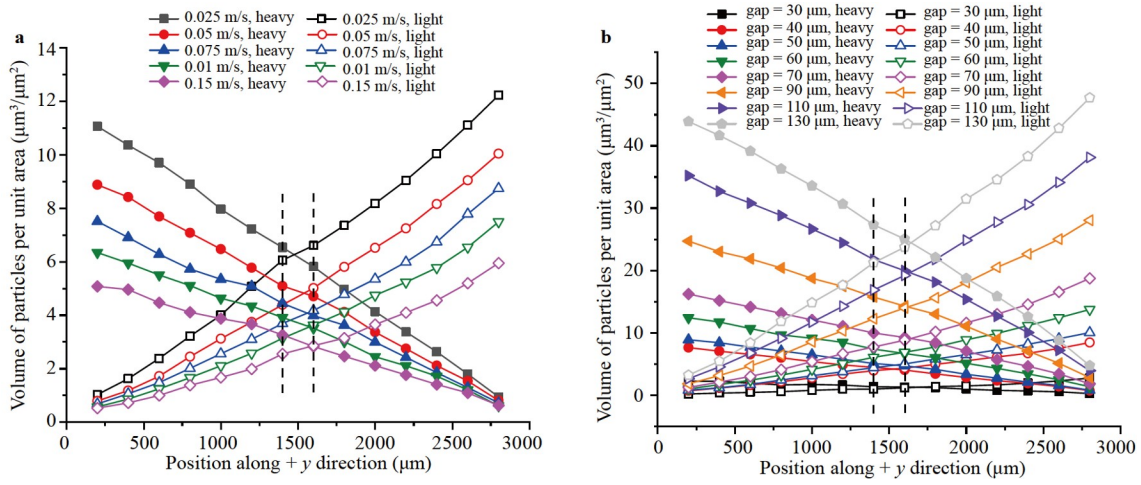

Figure 4 Variation in the volume of particles per unit area along the y direction for heavy and light particles: **a** with different spreading speeds; **b** with different layer gaps.

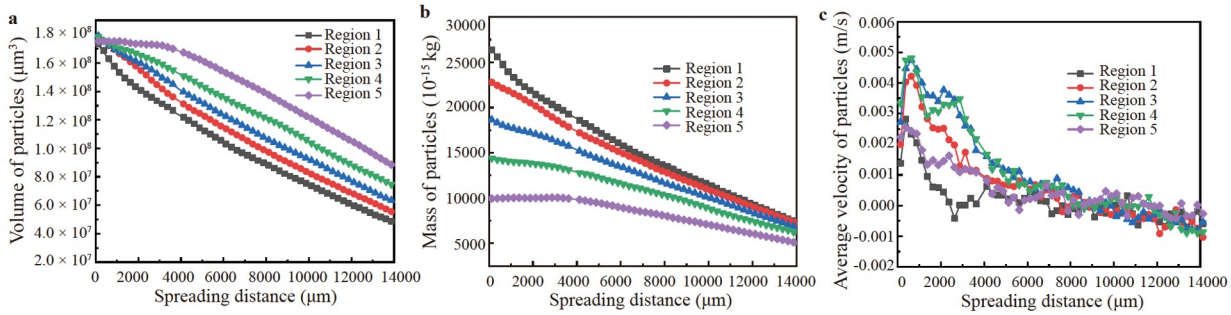

Figure 5 **a** Variation in the volume of particles in each section of the powder pile; **b** variation in the mass of each section of the powder pile; **c** variation in the average velocity of particles in each section of the powder pile.

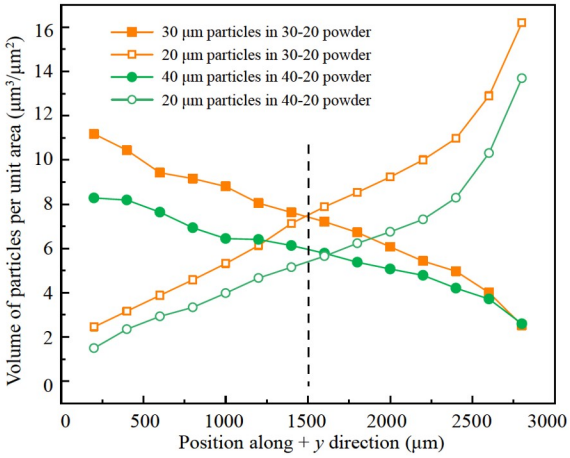

Figure 6 Variation in the deposited particle volume for heavy and light particles along the y direction when the spreading speed is 0.05 m/s and the layer gap is 70 μm.

graded powders, large particle size further enhances the diffusion of heavy particles. It is expected that to achieve a better distribution of graded powders in the y direction during the spreading, Ta powder should have a relatively smaller size distribution. In addition, the effect of the spreader design is also worth testing. As reported in Refs. [28,31], different spreader geometries can result in different deposited particle volumes in the powder layer. Future work is required to provide a feasible and controllable method to solve the issues related to the spreading of graded powders.

5. Conclusions

This work simulates the spreading of graded powders with large density differences (Ta and Ti particles with densities of 16.7 and 4.51 g/cm^3, respectively), and the effects of material density differences on the spreading performance are examined and explained. It is found that during the spreading of graded powders with the same particle size distribution but different densities, the volume of deposited particles on the heavy powder side (Ta) is slightly smaller than that on the light powder side (Ti), indicating the diffusion of heavy particles to the light particles. Such a diffusion phenomenon is affected by the spreading speed. With the spreading speed increasing, the deviation is more serious. The analysis also shows that the diffusion of particles from the heavy powder side to the light powder side mainly occurs at the beginning of the spreading and then stops after the steady state is reached. The examination of the effect of particle size reveals that larger particle size of heavy powder further enhances diffusion. It is suggested that decreasing the particle size of heavy powder may reduce diffusion.

Author contributions *Zongyan Zhou and Aibing Yu designed the research. Lin Wang wrote the first draft of the manuscript. Erlei Li and Baicheng Zhang helped organize the manuscript. Zongyan Zhou revised and edited the final version*

Acknowledgements *This work was supported by the Australian Research Council Industrial Transformation Research Hubs Scheme (Grant No. IH140100035), and undertaken with the assistance of resources from the National Computational Infrastructure (NCI), which is supported by the Australian Government.*

1 Y. Li, Z. Feng, L. Hao, L. Huang, C. Xin, Y. Wang, E. Bilotti, K. Essa, H. Zhang, Z. Li, F. Yan, and T. Peijs, A review on functionally graded materials and structures via additive manufacturing: From multi-scale design to versatile functional properties, Adv. Mater. Technol. **5**, 1900981 (2020).
2 C. Zhang, F. Chen, Z. Huang, M. Jia, G. Chen, Y. Ye, Y. Lin, W. Liu, B. Chen, Q. Shen, L. Zhang, and E. J. Lavernia, Additive manufacturing of functionally graded materials: A review, Mater. Sci. Eng.-A **764**, 138209 (2019).
3 G. H. Loh, E. Pei, D. Harrison, and M. D. Monzón, An overview of functionally graded additive manufacturing, Addit. Manuf. **23**, 34 (2018).
4 S. S. Wang, Fracture mechanics for delamination problems in composite materials, J. Compos. Mater. **17**, 210 (1983).
5 N. Noda, Thermal stresses in functionally graded materials, J. Thermal Stresses **22**, 477 (1999).
6 M. Naebe, and K. Shirvanimoghaddam, Functionally graded materials: A review of fabrication and properties, Appl. Mater. Today **5**, 223 (2016).
7 I. Gibson, D. W. Rosen, and B. Stucker, Additive Manufacturing Technologies (Springer, 2014).
8 L. Ren, Z. Song, H. Liu, Q. Han, C. Zhao, B. Derby, Q. Liu, and L. Ren, 3D printing of materials with spatially non-linearly varying properties, Mater. Des. **156**, 470 (2018).
9 B. Zhang, P. Jaiswal, R. Rai, and S. Nelaturi, Additive manufacturing of functionally graded material objects: A review, J. Comput. Inf. Sci. Eng. **18**, 041002 (2018).
10 W. E. Frazier, Metal additive manufacturing: A review, J. Mater. Eng. Perform. **23**, 1917 (2014).
11 T. D. Ngo, A. Kashani, G. Imbalzano, K. T. Q. Nguyen, and D. Hui, Additive manufacturing (3D printing): A review of materials, methods, applications and challenges, Compos. Part B-Eng. **143**, 172 (2018).
12 K. Essa, H. Hassanin, M. M. Attallah, N. J. Adkins, A. J. Musker, G. T. Roberts, N. Tenev, and M. Smith, Development and testing of an additively manufactured monolithic catalyst bed for HTP thruster applications, Appl. Catal. A-Gen. **542**, 125 (2017).
13 T. Niendorf, S. Leuders, A. Riemer, F. Brenne, T. Tröster, H. A. Richard, and D. Schwarze, Functionally graded alloys obtained by additive manufacturing, Adv. Eng. Mater. **16**, 857 (2014).
14 I. Maskery, N. T. Aboulkhair, A. O. Aremu, C. J. Tuck, I. A. Ashcroft, R. D. Wildman, and R. J. M. Hague, A mechanical property evaluation of graded density Al-Si10-Mg lattice structures manufactured by selective laser melting, Mater. Sci. Eng.-A **670**, 264 (2016).
15 S. Y. Choy, C. N. Sun, K. F. Leong, and J. Wei, Compressive properties of functionally graded lattice structures manufactured by selective laser melting, Mater. Des. **131**, 112 (2017).
16 N. Sudarmadji, J. Y. Tan, K. F. Leong, C. K. Chua, and Y. T. Loh, Investigation of the mechanical properties and porosity relationships in selective laser-sintered polyhedral for functionally graded scaffolds, Acta Biomater. **7**, 530 (2011).
17 M. Fousová, D. Vojtěch, J. Kubásek, E. Jablonská, and J. Fojt, Promising characteristics of gradient porosity Ti-6Al-4V alloy prepared by SLM process, J. Mech. Behav. BioMed. Mater. **69**, 368 (2017).
18 T. Traini, C. Mangano, R. L. Sammons, F. Mangano, A. Macchi, and

A. Piattelli, Direct laser metal sintering as a new approach to fabrication of an isoelastic functionally graded material for manufacture of porous titanium dental implants, Dent. Mater. **24**, 1525 (2008).
19 K. A. Mumtaz, and N. Hopkinson, Laser melting functionally graded composition of Waspaloy® and Zirconia powders, J. Mater. Sci. **42**, 7647 (2007).
20 H. Chung, and S. Das, Functionally graded Nylon-11/silica nanocomposites produced by selective laser sintering, Mater. Sci. Eng.-A **487**, 251 (2008).
21 V. E. Beal, P. Erasenthiran, N. Hopkinson, P. Dickens, and C. H. Ahrens, The effect of scanning strategy on laser fusion of functionally graded H13/Cu materials, Int. J. Adv. Manuf. Technol. **30**, 844 (2006).
22 C. Anstaett, C. Seidel, and G. Reinhart, in Fabrication of 3D multi-material parts using laser-based powder bed fusion: Proceedings of the 28th Annual International Solid Freeform Fabrication Symposium—An Additive Manufacturing Conference, Austin, 2017.
23 Y. Wen, B. Zhang, R. L. Narayan, P. Wang, X. Song, H. Zhao, U. Ramamurty, and X. Qu, Laser powder bed fusion of compositionally graded CoCrMo-Inconel 718, Addit. Manuf. **40**, 101926 (2021).
24 P. A. Cundall, and O. D. L. Strack, A discrete numerical model for granular assemblies, Géotechnique **29**, 47 (1979).
25 C. Kloss, C. Goniva, A. Hager, S. Amberger, and S. Pirker, Models, algorithms and validation for opensource DEM and CFD-DEM, Prog. Comput. Fluid Dyn. **12**, 140 (2012).
26 S. Plimpton, Fast parallel algorithms for short-range molecular dynamics, J. Comput. Phys. **117**, 1 (1995).
27 L. Wang, E. L. Li, H. Shen, R. P. Zou, A. B. Yu, and Z. Y. Zhou, Adhesion effects on spreading of metal powders in selective laser melting, Powder Tech. **363**, 602 (2020).
28 L. Wang, A. Yu, E. Li, H. Shen, and Z. Zhou, Effects of spreader geometry on powder spreading process in powder bed additive manufacturing, Powder Tech. **384**, 211 (2021).
29 R. Everaers, and M. R. Ejtehadi, Interaction potentials for soft and hard ellipsoids, Phys. Rev. E **67**, 041 (2003).
30 H. Chen, Q. Wei, Y. Zhang, F. Chen, Y. Shi, and W. Yan, Powder-spreading mechanisms in powder-bed-based additive manufacturing: Experiments and computational modeling, Acta Mater. **179**, 158 (2019).
31 S. Haeri, Optimisation of blade type spreaders for powder bed preparation in Additive Manufacturing using DEM simulations, Powder Tech. **321**, 94 (2017).

粉末床熔融的多材料铺粉过程中粉末扩散的数值研究

王林, 李二垒, 周宗彦, 张百成, 余艾冰

摘要 粉末床熔融增材制造技术已应用于功能梯度材料的制造. 文献中报道了一种材料成分沿垂直于粉末铺粉方向变化的新设计. 基于此设计, 本工作采用离散单元数值模拟研究了两种密度差异较大的金属粉末在铺粉过程中颗粒的偏析情况. 结果发现, 在铺粉过程中, 较大密度粉末(重颗粒)一侧的铺粉量小于较小密度粉末(轻颗粒)的一侧的铺粉量. 这种现象表明重颗粒从粉末密度大的一侧向粉末密度较小的一侧扩散. 这种扩散受铺粉速度影响较大, 铺粉速度越快, 扩散越明显. 但粉末层厚度对扩散影响不大. 结果还表明, 重颗粒与轻颗粒间的粒径差异影响扩散较大, 减小重颗粒的粒径可能是控制颗粒偏析的一种方案.